nature structural & molecular biology

One-way membrane trafficking of SOS in receptor-triggered Ras activation

Sune M Christensen[1,5,6], Hsiung-Lin Tu[1,5,6], Jesse E Jun[2,6], Steven Alvarez[1], Meredith G Triplet[1], Jeffrey S Iwig[3], Kamlesh K Yadav[4,5], Dafna Bar-Sagi[4], Jeroen P Roose[2,7] & Jay T Groves[1,7]

SOS is a key activator of the small GTPase Ras. In cells, SOS-Ras signaling is thought to be initiated predominantly by membrane recruitment of SOS via the adaptor Grb2 and balanced by rapidly reversible Grb2-SOS binding kinetics. However, SOS has multiple protein and lipid interactions that provide linkage to the membrane. In reconstituted-membrane experiments, these Grb2-independent interactions were sufficient to retain human SOS on the membrane for many minutes, during which a single SOS molecule could processively activate thousands of Ras molecules. These observations raised questions concerning how receptors maintain control of SOS in cells and how membrane-recruited SOS is ultimately released. We addressed these questions in quantitative assays of reconstituted SOS-deficient chicken B-cell signaling systems combined with single-molecule measurements in supported membranes. These studies revealed an essentially one-way trafficking process in which membrane-recruited SOS remains trapped on the membrane and continuously activates Ras until being actively removed via endocytosis.

Ras is a membrane-anchored small GTPase that plays a central role in many signaling pathways. Ras can exist in an inactive (GDP-bound) or active (GTP-bound) state. Ras activation is mediated by a variety of Ras guanine-nucleotide-exchange factors (RasGEFs) that catalyze the exchange of Ras-bound nucleotide with cytoplasmic GTP[1–3]. This process is opposed by Ras-GTPase-activating proteins (RasGAPs) that enhance the intrinsic GTPase activity of Ras and thus promote Ras deactivation[1]. Ras activation must be tightly regulated; aberrant activation of Ras is responsible for many human cancers[4].

Son of Sevenless (SOS) is a widely distributed RasGEF[5–7] whose full activation through an allosteric mechanism results in digital (i.e., bimodal) patterns of receptor-induced Ras kinase signaling[8,9]. The activation of Ras by SOS is critical for diverse processes such as cell growth[10], T-cell activation and development[8,9,11,12], early B-cell development[13], embryogenesis[14], and differentiation of embryonic stem cells[15].

Receptor-triggered activation of SOS is a multilayered process involving membrane recruitment, release of autoinhibition, and allosteric modulation by Ras. The initial membrane recruitment of SOS is thought to occur via association of PxxP motifs in the C-terminal proline-rich (PR) domain with Grb2, which in turn binds phosphotyrosine motifs on activated receptors or transmembrane adaptor proteins[6,7,10,16–21]. SOS additionally contains a series of N-terminal domains with Dbl homology (DH) and pleckstrin homology (PH) as well as a histone-fold (HF) domain (**Fig. 1a**), which autoinhibits SOS activity when assayed in solution. On membranes, this autoinhibition is released through interactions with various membrane lipids[22–24] (reviewed in ref. 9). Full activation of SOS is contingent on binding of Ras to an allosteric pocket situated at the rim of the REM and CDC25 domains[25]. The REM and CDC25 domains in SOS1 together form the catalytic core, which we denote SOS^{Cat} herein (**Fig. 1a**). Mutations in *SOS1* that perturb these regulatory functions result in altered signaling behavior and have been implicated in developmental disorders such as Noonan[26], Costello, and CFC syndromes[27]. SOS2 has a very similar domain makeup but appears to be somewhat redundant with SOS1 in cells[13]; in this study, we focused solely on SOS1.

Historically, SOS activation has been rationalized in terms of a simple membrane-recruitment model based on substrate accessibility (**Fig. 1b**). Grb2 binding to activated receptors recruits the SOS–Grb2 complex from the cytosol, thereby positioning SOS in proximity to membrane-anchored Ras and consequently promoting nucleotide exchange[5,28]. However, the importance of Grb2-mediated membrane recruitment is challenged by observations that truncated SOS constructs lacking the PR domain still localize to the membrane after receptor stimulation and are fully signaling competent or even exhibit increased responsiveness compared with that of the full-length enzyme[29–34]. Recent work with mouse embryonic stem cells[15] has demonstrated that, beyond Grb2-facilitated membrane recruitment, SOS activity is governed by a combination of weak-to-moderate

[1]Department of Chemistry, University of California, Berkeley, Berkeley, California, USA. [2]Department of Anatomy, University of California, San Francisco, San Francisco, California, USA. [3]Howard Hughes Medical Institute, Department of Molecular and Cell Biology, University of California, Berkeley, Berkeley, California, USA. [4]Department of Biochemistry, New York University School of Medicine, New York, New York, USA. [5]Present addresses: Novozymes A/S, Bagsvaerd, Denmark (S.M.C.), Institute for Molecular Engineering, University of Chicago, Chicago, Illinois, USA (H.-L.T.) and Department of Urology, Icahn School of Medicine at Mount Sinai, New York, New York, USA (K.K.Y.). [6]These authors contributed equally to this work. [7]These authors jointly supervised this work. Correspondence should be addressed to J.P.R. (jeroen.roose@ucsf.edu) or J.T.G. (jtgroves@lbl.gov).

Received 5 February; accepted 8 July; published online 8 August 2016; doi:10.1038/nsmb.3275

protein-protein and protein-lipid interactions mediated by the multiple domains of SOS[15,24,33,35]. These studies suggest that the recruitment to membrane integral receptors via Grb2 is an oversimplified model for SOS function (**Supplementary Note 1**).

We observed that SOS constructs lacking the Grb2-binding PR domain are successfully recruited to reconstituted Ras-functionalized membranes through Ras- and lipid-binding interactions. Additionally, using a micropatterned fluid supported-lipid-bilayer platform[36,37] in which the catalytic activity of individual SOS molecules can be directly resolved[38], we found that a single SOS molecule has the capacity to processively activate thousands of Ras proteins during a single membrane residency period (**Fig. 1c**,**d**). Such high degrees of processivity and essentially irreversible membrane recruitment in the activation of Ras by SOS have not been captured in earlier mechanistic and computational models of SOS activity, or in synthetic-biology approaches using Grb2-SOS1 fusion proteins[8,15].

Does such extreme processivity of SOS occur in cells, and, if so, how it is regulated? To address this question, we mapped the individual contributions of the different domains of SOS1 to membrane association, through a series of single-molecule dwell-time measurements and bulk kinetic observations. These studies used a reconstituted-membrane system in combination with quantitative cell-based signaling assays (details in **Supplementary Note 1**). Altogether, our results reveal an essentially one-way trafficking process in which membrane-recruited SOS1 remains trapped on the membrane and continuously activates Ras until being actively removed, such as by endocytosis. This mechanism differs substantially from the reversible Grb2-dependent process that has been generally assumed[6,7,10,16–19]. The Ras-activation machinery may remain active or be inactivated regardless of the triggering state of the receptor that initiated the signal; this phenomenon substantially affects the quantitative input-response function for Ras activation by receptor triggering and underscores the importance of strong inhibition of spontaneous SOS activation.

RESULTS

Supported-lipid-bilayer SOS-activation assay

We developed an imaging assay to study the interaction of SOS with Ras on supported lipid bilayers (SLBs; **Fig. 2a**). In this experimental configuration, we coupled H-Ras (residues 1–181, C118S mutant, henceforth referred to as Ras) to the bilayer at C181 via a maleimide-functionalized lipid (Online Methods), thus yielding permanently bound and laterally mobile Ras that was fully functional with respect to SOS activity[22,38,39] (**Supplementary Fig. 1a**). A calibration curve obtained with fluorescence correlation spectroscopy provided access to the local surface density of Ras via epifluorescence imaging of Ras-bound fluorescent nucleotide labels (GDP- and GTP-BODIPY; **Supplementary Fig. 1b** and ref. 38). Labeling of SOS with a photostable and bright fluorophore (ATTO 647N) facilitated reliable counting and tracking of individual SOS molecules at the membrane surface by total internal reflection fluorescence microscopy (TIRFM). Control experiments showed that labeling did not perturb the observed activity of SOS (**Supplementary Fig. 1c**).

In this system, we initiated measurements by flowing purified SOS1 over the Ras-functionalized SLBs in a transient pulse with a defined concentration profile (**Fig. 2a**). During such a pulse, SOS1 interacts with membrane-bound Ras and, in the absence of free nucleotide in solution, becomes trapped after binding Ras at the catalytic site[30,40]. This method provided a convenient means of quantifying the probability of SOS1 engaging Ras by directly counting the number of SOS1 molecules remaining at the bilayer after a pulse (**Fig. 2b** and Online Methods). Chasing with unlabeled nucleotide initiated the exchange reaction and resulted in processive (i.e., sustained) turnover of Ras by the recruited and successfully activated SOS1 molecules (**Fig. 2a** and **Supplementary Fig. 1d**). A constant flow during the experiment ensured that dissociated SOS1 was removed from the reaction chamber, thus permitting measurement of the desorption kinetics.

Allosteric activation of SOS via altered membrane recruitment

An important functional aspect of SOS1 in the cellular context is its activation by RasGTP binding to an allosteric site, located between the CDC25 and Ras-exchanger motif (REM) domains in the catalytic core, termed SOS^{Cat} (ref. 25). This allosteric activation sensitively depends on the nucleotide state of Ras[41] and is thought to enable a RasGTP positive feedback loop operating at the membrane[8,9].

Allosteric binding of Ras by SOS also provides an alternate mechanism to recruit SOS to the membrane. Here, we first quantitatively analyzed recruitment by examining the SOS^{Cat} module, which contains both the active site and the allosteric Ras-binding pocket but lacks any lipid-binding domains[25]. SOS^{Cat} was recruited to the Ras bilayer during the pulse phase of the assay (**Fig. 2c**). The known concentration profile of SOS^{Cat} during the pulse, combined with locally measured Ras densities, permitted quantification of the recruitment probability from the adsorption traces (i.e., the probability of a SOS^{Cat} molecule being trapped after collision with Ras at the membrane (**Fig. 2d** and Online Methods)).

We found that membrane recruitment of SOS^{Cat} was sensitive to the nucleotide state of Ras, observing an ~16-fold enhancement on SLBs displaying RasGTP (**Fig. 2d**). A Y64A point mutation in Ras, previously shown to abolish Ras binding to the catalytic site of SOS[42], resulted in only transient recruitment of SOS^{Cat}, thus demonstrating that, as expected, SOS is trapped at the membrane after binding Ras at the catalytic site in the absence of free nucleotide (**Fig. 2c**). Nucleotide-dependent recruitment was preserved for Ras^{Y64A}, thus indicating that the allosteric binding pocket is the primary determinant of this property of SOS^{Cat} (**Fig. 2d**). A W729E point mutation in SOS1, known to prevent binding of allosteric Ras[8,43], essentially abrogated recruitment (**Fig. 2c**,**d**). After chasing with nucleotide, a population of highly processive SOS^{Cat} remained at the membrane (tail of the curve in **Fig. 2c**), which we identified as successfully activated SOS^{Cat} molecules. The long-lived (minute-to-hour scale) membrane-bound SOS^{Cat} was catalytically active (**Supplementary Fig. 1d** and ref. 38), thus indicating that release of SOS from the membrane was predominantly limited by the allosterically bound Ras.

We substantiated our findings in the SLB experiments with cellular assays (**Supplementary Note 2** and **Supplementary Fig. 2a–d**). Collectively, the data demonstrated a distinct positive allosteric effect of RasGTP at the stage of membrane recruitment. These results, together with the insensitivity of the average specific activity of SOS to the nucleotide state of Ras[38], indicated that RasGTP-mediated recruitment of SOS via its allosteric site is one mechanism by which the well-known accelerating effect of RasGTP on SOS mediated Ras activation is achieved (commonly referred to as positive feedback)[8,22,41].

Regulation of membrane binding by N-terminal domains

It is not known whether membrane recruitment and retention of SOS^{Cat} are influenced by its flanking lipid-binding domains. At the N-terminal side, the catalytic core of SOS1 is flanked by a DH-PH cassette and an HF domain (**Fig. 3a**). Structural and biochemical studies have shown that the N-terminal domains exert an autoinhibitory effect on SOS1 activity, presumably through steric obstruction of the

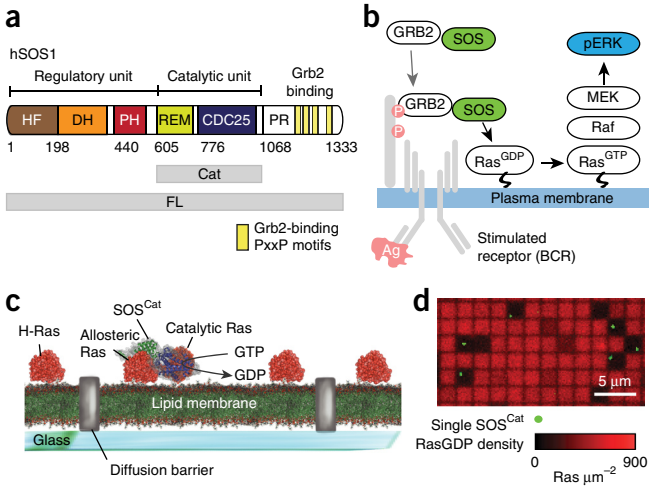

Figure 1 The catalytic core of SOS is stably and functionally recruited to Ras-decorated SLBs *in vitro*, independently of Grb2 and lipid-binding domains. (**a**) The domain architecture of full-length (FL) hSOS1. The catalytic unit (Cat) is depicted together with the flanking regulatory domains. Yellow boxes in the C-terminal PR domain indicate PxxP motifs, which interact with Grb2. (**b**) Classical model of the SOS-Ras-ERK signal-transduction pathway. In the shown example, SOS is recruited to the plasma membrane downstream of activated B-cell receptors via binding of Grb2 to phosphotyrosine motifs on the adaptor protein LAB. (**c**) Single SOS activity assay based on micropatterned Ras-functionalized fluid SLBs. (**d**) Representative overlay image of fluorescent GDP bound to Ras (red channel) and membrane-recruited SOS^{Cat} (green channel) in the single-molecule assay depicted in **c**. Darker areas with depleted signal in the GDP channel indicate membrane corrals to which individual copies of SOS^{Cat} were recruited and exhibited highly processive SOS^{Cat} activity, activating Ras in a sustained manner without dissociating from the membrane surface. This experiment was repeated five times.

allosteric Ras-binding pocket, as observed in crystal structures[23,43]. The PH domain interacts with phosphatidylinositol 4,5-bisphosphate (PIP_2) lipids[35,44] and phosphatidic acid[33], and the HF domain contains several additional interaction sites for negatively charged lipids[23,24]. These lipid interactions are generally believed to play a role in the release of autoinhibition, but the underlying mechanisms are unclear.

We observed a pronounced damping effect on initial membrane recruitment of SOS1 after adding the N-terminal domains to SOS^{Cat}. Appending the DH-PH unit to the catalytic core (SOS^{DPC}) reduced recruitment to the membrane by approximately three-fold. Inclusion of the full N terminus (construct comprising HF-DH-PH-Cat domains (SOS^{HDPC})) damped recruitment by ~66-fold relative to that of SOS^{Cat} (**Fig. 3b**). Even in the case of the highly autoinhibited HDPC construct, Ras-specific binding was evident (**Supplementary Fig. 2e**). These observations clearly demonstrated that a major property of the N terminus is the down-modulation of spontaneous SOS1 activation by hindering its initial recruitment to the membrane, as evidenced by the steric hindrance of the allosteric Ras-binding site observed in structures[23,43]. Interestingly, a gain-of-function R552G point mutation associated with Noonan syndrome ($SOS^{HDPC\ R552}$)[6], compared with SOS^{HDPC}, caused a slight relief of such inhibition (**Fig. 3b** and **Supplementary Fig. 3a**), thus emphasizing the importance of a tightly regulated membrane recruitment step. As observed for SOS^{Cat} (**Fig. 2c**,**d**), the longer constructs also exhibited increased recruitment on bilayers displaying RasGTP (**Supplementary Fig. 3a**).

Although the N-terminal domains inhibited initial recruitment, SOS^{DPC} and SOS^{HDPC} exhibited extremely long dwell times on Ras-functionalized bilayers (with a mean residency period on the hour scale; **Fig. 3c**, **Supplementary Fig. 3b**,**c** and Online Methods). The N-terminal domains thus mediate two major functions: inhibition of the initial recruitment probability and enhancement of the dwell time in the active membrane-bound state. This anticorrelation between membrane recruitment probability and dwell time gives rise to an interesting dual functionality in which rare activation events are coupled to a potent response (**Supplementary Fig. 3d**,**e**).

Multicomponent analysis of SOS-Ras-ERK signaling

To establish the effects of intrinsic chemical SOS1 properties—as determined from reconstituted-SLB assays—on cellular SOS1-Ras signaling, we optimized a SOS1- and SOS2-double-deficient ($SOS1^{-}2^{-}$) DT40 chicken B-cell system that we have previously used to characterize digital SOS1-Ras-MAPK ERK signal transduction after B-cell receptor (BCR) ligation[8,45,46]. Here, we introduced

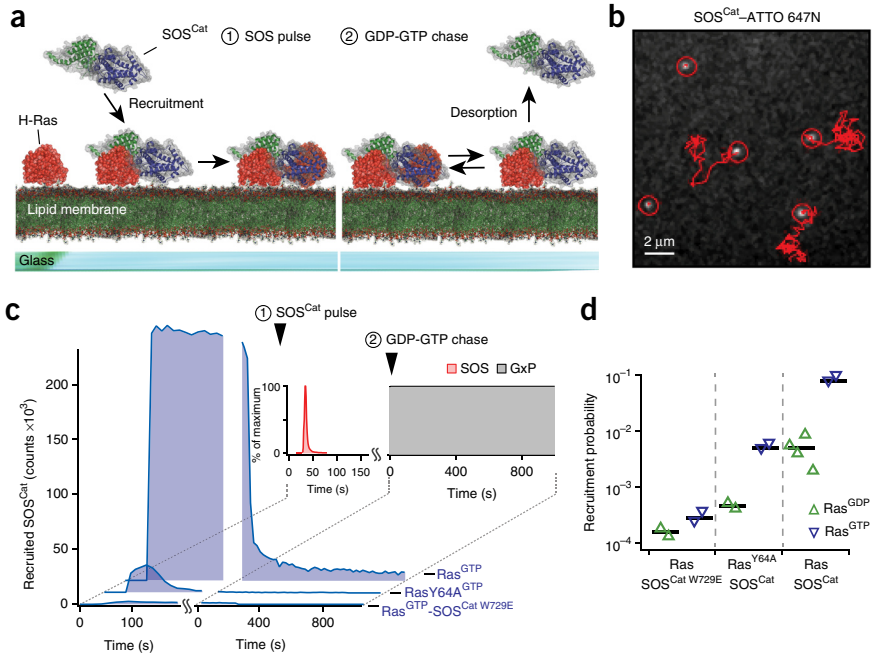

Figure 2 Stopped-flow SLB assay probing SOS recruitment and desorption. (**a**) Cartoon representation of the two phases of the assay. (**b**) Single-molecule tracking of ATTO 647N–labeled SOS^{Cat} diffusing at the bilayer. (**c**) Traces from the stopped-flow assay. Experiments used SOS^{Cat}; $SOS^{Cat\ W729E}$, a mutant with an abolished allosteric pocket; and Ras^{Y64A}, a construct deficient in binding to the active site of SOS. The indicated counts are for a field of view of 55 × 55 µm^2 and were scaled according to the applied ratio of unlabeled to labeled enzymes. (**d**) Membrane recruitment probabilities quantified from phase 1 of the stopped-flow assay. Each triangle represents data from a SLB sample. Black horizontal lines indicate the average of the data shown for each condition. Source data for plots and graphs are available online.

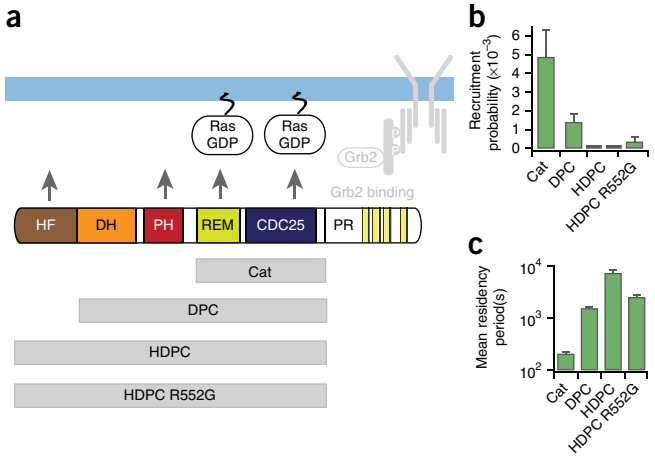

Figure 3 The N terminus of SOS suppresses bilayer recruitment while prolonging dwell time in the active membrane-bound state. (**a**) SOS constructs tested in the stopped-flow SLB assay. All experiments shown were conducted with RasGDP on the bilayer. (**b**) Recruitment probability of SOS constructs obtained from the stopped-flow assay. Each bar represents the average of data collected for the following number of SLB samples, except for HDPC, for which each bar reflects data from one SLB: SOS^{Cat}, $n = 4$; DPC, $n = 4$; HDPC, $n = 2$; HDPC R552G, $n = 3$. Each sample was imaged in at least 15 different positions. Error bars, s.e.m. (data for SOS^{Cat} are replotted from **Figure 2** for comparison). (**c**) Membrane residence time of SOS constructs obtained from the stopped-flow assay. The mean residency period for each construct was obtained by fitting desorption traces (**Supplementary Fig. 3b**) from the following number of SLB samples: SOS^{Cat}, $n = 5$; DPC, $n = 4$; HDPC, $n = 2$; HDPC R552G, $n = 3$. Error bars, estimated s.d. of the fit coefficient for an average over the indicated samples. Source data for plots and graphs are available online.

EGFP-tagged variants of human SOS1 (hSOS1) into these cells entirely devoid of endogenous SOS1 and SOS2, left the cells unstimulated or induced BCR ligation, and monitored EGFP-SOS localization by fluorescence microscopy or activation of the ERK kinase by using an antibody to phospho-ERK (pERK) and flow cytometry[8,46] (**Fig. 4a**,**b**). The latter experimental platform, henceforth denoted the p-FLOW assay (Online Methods), revealed the quantitative magnitudes of Ras-ERK responses at the individual-cell level along with SOS1 expression levels. We depicted 3D representations of the data by mapping the time evolution of pERK after BCR stimulation as a function of SOS1 expression level (**Fig. 4c**,**d**). pERK traces corresponding to specific SOS1 levels represent 2D slices through the data (**Fig. 4f**,**g**,**i**,**j**).

Timely signaling requires SOS^{Cat} flanking domains

Transient transfection of EGFP-tagged full-length human SOS1 (SOS^{FL}) rescued the characteristic BCR-induced pERK patterns in SOS-deficient DT40 cells (**Fig. 4b** and **Supplementary Fig. 4a**,**b**).

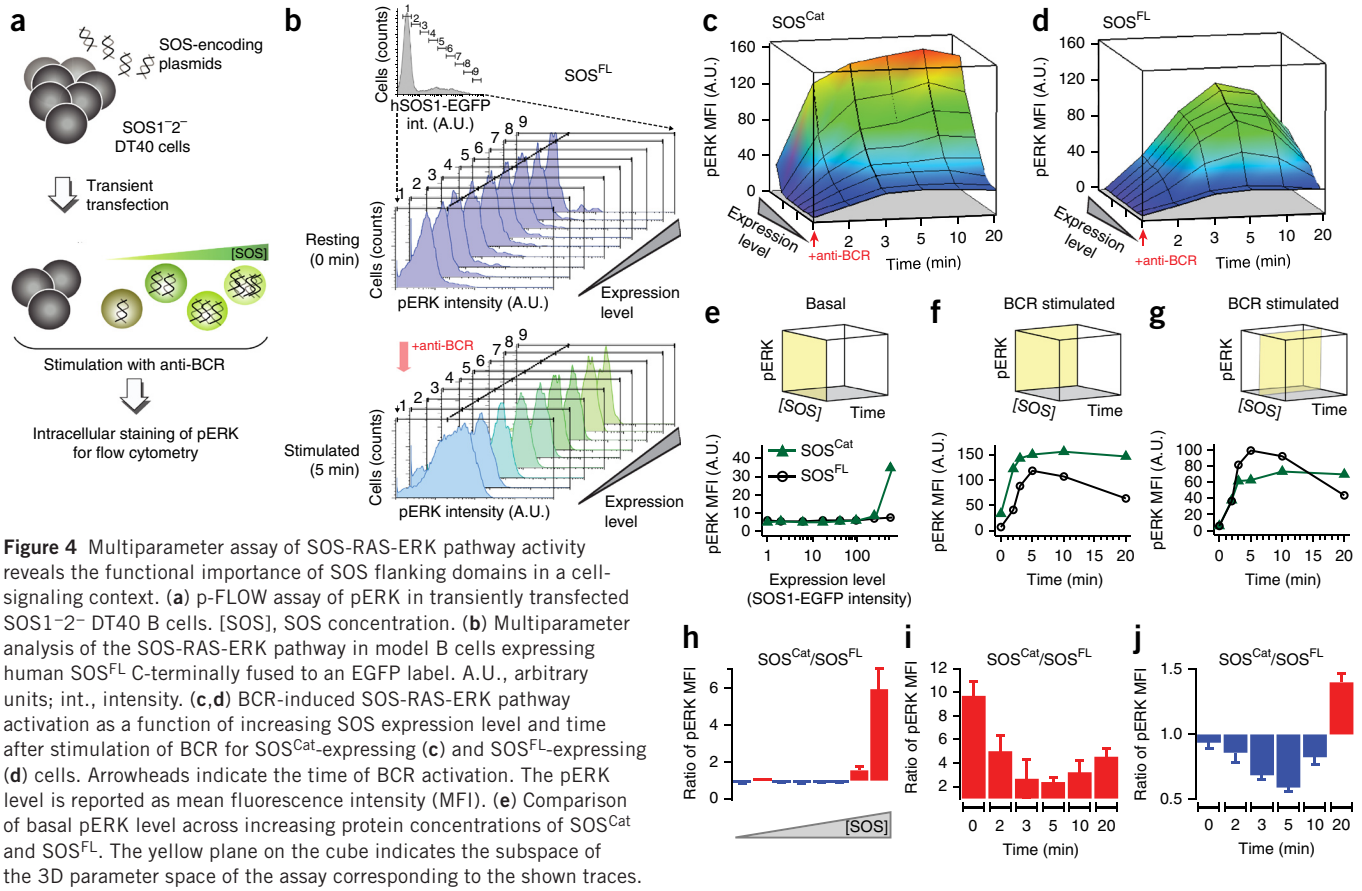

Figure 4 Multiparameter assay of SOS-RAS-ERK pathway activity reveals the functional importance of SOS flanking domains in a cell-signaling context. (**a**) p-FLOW assay of pERK in transiently transfected SOS1⁻2⁻ DT40 B cells. [SOS], SOS concentration. (**b**) Multiparameter analysis of the SOS-RAS-ERK pathway in model B cells expressing human SOS^{FL} C-terminally fused to an EGFP label. A.U., arbitrary units; int., intensity. (**c**,**d**) BCR-induced SOS-RAS-ERK pathway activation as a function of increasing SOS expression level and time after stimulation of BCR for SOS^{Cat}-expressing (**c**) and SOS^{FL}-expressing (**d**) cells. Arrowheads indicate the time of BCR activation. The pERK level is reported as mean fluorescence intensity (MFI). (**e**) Comparison of basal pERK level across increasing protein concentrations of SOS^{Cat} and SOS^{FL}. The yellow plane on the cube indicates the subspace of the 3D parameter space of the assay corresponding to the shown traces. (**f**,**g**) Comparative plots representing the dynamic change in BCR-induced pERK as a function of stimulation time in cells expressing superphysiological levels (**f**) and intermediate levels (**g**) of SOS^{Cat} and SOS^{FL}. (**h**–**j**) Ratios of pERK observed in SOS^{Cat}- and SOS^{FL}-transfected cells, corresponding to traces in **e**–**g**. Red fill indicates increased activity of SOS^{Cat} as compared to SOS^{FL}, whereas blue fill highlights decreased relative activity. Data are based on seven independent cell cultures and p-FLOW experiments. Error bars, s.e.m. Source data for plots and graphs are available online.

SOS^{Cat}, lacking the Grb2-binding domain as well as the N-terminal lipid-interacting domains, triggered Ras-ERK signaling patterns that differed substantially from those triggered by SOS^{FL} (**Fig. 4c**,**d** and **Supplementary Fig. 4c**,**d**). Cells expressing high levels of SOS^{Cat}, compared with cells expressing SOS^{FL}, exhibited more spontaneous activation of ERK in the absence of receptor stimulation (**Fig. 4e**,**h**). Even under these conditions, BCR stimulation further increased ERK activation in SOS^{Cat}-containing cells (**Fig. 4c**,**f**,**i**). Another notable difference was the signal attenuation. Whereas SOS^{FL}-induced pERK signals decreased at later time points after BCR stimulation (10–20 min.), SOS^{Cat} continued to signal in a sustained manner, and SOS^{Cat} outperformed SOS^{FL} (**Fig. 4f**,**i**). The sustained signaling from SOS^{Cat} cells suggests that the essentially irreversible membrane anchoring of SOS^{Cat} observed in reconstituted assays may exist in cells as well, but not for SOS^{FL}.

Domains flanking SOS^{Cat} might initially appear to merely dampen signal output. However, selective examination of cells expressing intermediate SOS levels revealed that SOS^{FL} signaled more efficiently than SOS^{Cat} in response to BCR stimulation (**Fig. 4g**,**j**). Moreover, this intermediate SOS^{FL} level resulted in rescued pERK responses that were nearly identical to those observed for wild-type DT40 cells, thus suggesting that reconstitution with intermediate hSOS1 levels matches the physiological level expressed in wild-type DT40 cells (**Supplementary Fig. 4b**). The data revealed that domains flanking SOS^{Cat} have both positive and negative regulatory roles.

SOS autoinhibition prevents spontaneous activation

A number of structural and cellular studies have established regulatory mechanisms that affect SOS1 activity, but several proposed mechanisms appear to be contradictory[22–24,43]. To understand how

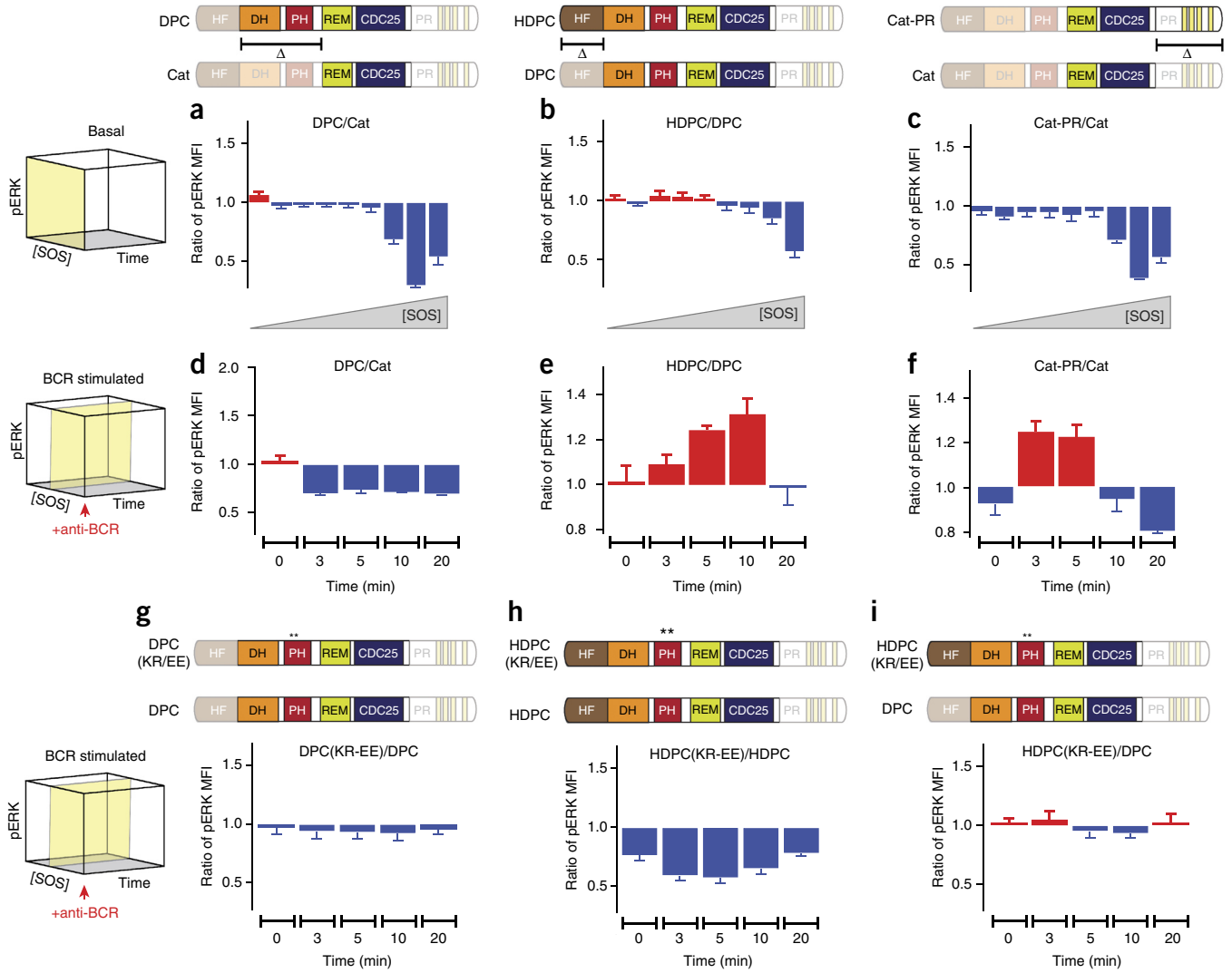

Figure 5 SOS^{Cat} flanking domains block spontaneous activation in the basal state but promote RAS-ERK signal transduction after receptor stimulation. (**a**–**c**) p-FLOW assays showing inhibition of spontaneous ERK activation after addition of SOS^{Cat} flanking domains: DH-PH domain (**a**), HF domain (**b**), and PR domain (**c**) (depicted schematically in domain diagrams at the top). The ratio of pERK MFI for longer to shorter SOS variants is plotted against increasing SOS concentration for unstimulated cells (basal state). (**d**–**f**) Time dependence of the pERK MFI ratio after BCR stimulation, plotted for the DH-PH domain (**d**), HF domain (**e**), and PR domain (**f**) (depicted schematically in domain diagrams at the top). (**g**–**i**) Comparison of BCR-induced ERK activation in the KR-EE PH-domain mutant (**) and wild-type SOS1 variants, showing disruption of membrane lipid interaction in the KR-EE mutant. Yellow planes on the cubes to the left indicate the corresponding subspace of the 3D parameter space in the p-FLOW assay (c.f. **Fig. 4c**,**d**). Data are based on three independent experiments. Error bars, s.e.m. Source data for plots and graphs are available online.

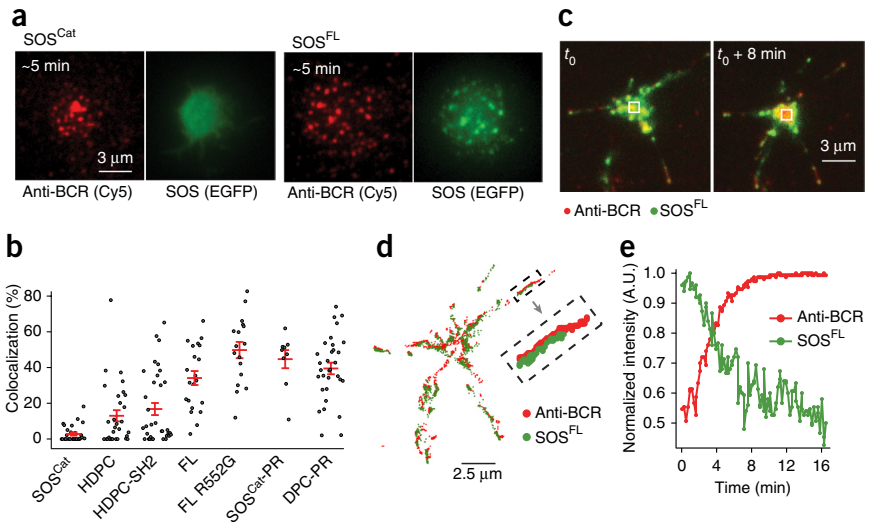

Figure 6 PR-domain-dependent localization of SOS to BCR microclusters and SOS depletion from the central BCR cluster formed between B cells and SLBs decorated with BCR-cross-linking antibody. (**a**) Representative TIRFM images illustrating spatial localization of SOS and BCR microclusters. Cells expressing SOS^{Cat} (left) and SOS^{FL} (right) at an early (~5-min) time point after contacting the bilayer are shown. The number of replicates is given in **b**. (**b**) Colocalization of different SOS variants and BCR microclusters. Each dot on the graph represents data from one cell. Red horizontal lines indicate average ± s.e.m. for the shown scatter data. Numbers of cells/SLB samples are: SOS^{Cat}, 28/5; HDPC, 30/2; HDPC-SH2, 34/2; FL, 21/2; FL R552G, 17/2; SOS^{Cat}-PR, 9/2; DPC-PR, 32/1. (**c**) Overlay of anti-BCR (Cy5, red) and SOS (EGFP, green) fluorescence signals before (left) and after (right) the formation of a central BCR cluster. The displayed overlays are also plotted as separate image channels in **Supplementary Figure 7c**. (**d**) Trajectories of BCR (red) and SOS^{FL} (green) movement at the cell-bilayer interface. The trajectories were obtained by tracking individual BCR and SOS clusters in a time lapse (**Supplementary Movie 1**) of the cell shown in **c**. Each tracked position of a microcluster is indicated by a dot. Chains of connected dots draw out microcluster trajectories. (**e**) Normalized time traces of the fluorescence intensity of SOS^{FL}-EGFP and BCR at the center of the cell-supported bilayer synapse for the cell shown in **c**. The phenomenon of SOS depletion from the central BCR cluster was observed in 69% of SOS^{FL}-expressing cells (95 cells imaged over five experiments). Source data for plots and graphs are available online.

SOS1 restricts spontaneous signaling in cells yet allows for controlled allosteric activation near the membrane interface, we first focused on SOS^{Cat} flanking domains in the basal state (**Fig. 5a–c**), i.e., in resting cells[6,7].

Addition of N-terminal domains to SOS^{Cat} blocked the spontaneous activation of Ras-ERK in cells expressing high levels of SOS (**Fig. 5a**,**b** and **Supplementary Fig. 5a–d**). The inhibitory potential scaled in an incremental manner with the number of domains flanking the catalytic core; i.e., SOS^{DPC} signaling was more restrained than SOS^{Cat} signaling (**Fig. 5a**), and SOS^{HDPC} was more inhibited than SOS^{DPC} (**Fig. 5b**). These results corroborate the SLB results in **Figure 3b**. Structural and biochemical studies on SOS1 demonstrated that the DH domain limits Ras binding at the allosteric pocket, and without removal of DH-mediated autoinhibition and allosteric activation, the catalytic pocket cannot fully accommodate RasGDP or dislodge GDP from Ras[22,43]. The HF strengthens SOS autoinhibition by blocking allosteric activation and by stabilizing a closed conformation of SOS[23,47]. These structural findings are consistent with our p-FLOW results for the resting cell state (**Fig. 5a–c**). Notably, despite considerable effort, it has not been feasible to purify functional full-length SOS1 including the PR domain, thus preventing its examination in our earlier SLB assays[38].

The C-terminal PR domain is most noted for its positive regulatory role in connecting SOS to activated receptors via Grb2. Grafting only the PR domain onto SOS^{Cat} revealed an inhibitory effect of this domain in restricting ligand-independent activation of SOS1 (**Fig. 5c**); this effect was independent of the autoinhibitory effect of the HF and DH-PH domains. The magnitude of inhibition conferred by the PR domain was comparable to that of the DH-PH domain relative to SOS^{Cat} (**Fig. 5a**,**c**), thus demonstrating that the N- and C-terminal domains have similar potency in curbing the activity of the catalytic SOS^{Cat} core in resting cells.

Positive regulation of SOS activity in stimulated cells

Next we investigated SOS1 regulation in BCR-stimulated cells expressing intermediate SOS1-EGFP levels (**Fig. 5d–f**). It has been reported that autoinhibition by the DH domain can be released by electrostatic interaction of the PH domain with membrane lipids, thus allowing allosteric Ras binding[15,22,33]. In our p-FLOW assay, we found that the DH-PH domain alone had a purely inhibitory effect relative to that of SOS^{Cat} under conditions of BCR stimulation (**Fig. 5d**). In contrast with inclusion of the DH-PH, inclusion of the HF domain in SOS^{DPC} resulted in increased signaling output (**Fig. 5e**). We also observed a positive regulatory role of HF after BCR stimulation for SOS containing the PR domain (**Supplementary Fig. 5e–g**). These findings are in agreement with the *in vitro* observation that HF enhances the residence time of membrane-recruited SOS (**Fig. 3c**).

For the DH-PH, our results from stimulated cells conflicted with the increased dwell time observed in the SLB assays (**Fig. 3c**). The inhibitory effect of DH-PH was unexpected because PH-lipid interaction has been reported to positively regulate GTP loading of Ras in COS-1 cells and in mouse embryonic-stem-cell differentiation[15,22,33]. This disparity may arise from the HF truncation counteracting the phospholipid binding of PH in the cell system. To test this possibility, we introduced combined mutation of K456E and R459E (KR-EE mutation) within the PH domain, thereby disrupting the PIP_2-PH interaction[15,35], and compared the BCR-stimulated ERK activation associated with the mutant and wild-type SOS1 variants (**Fig. 5g–i**). The KR-EE mutation in DPC format had a relatively small effect, resulting in a small decrease in pERK (**Fig. 5g**). However, the KR-EE mutation in HDPC markedly antagonized SOS1 activation throughout the entire assay duration, thus supporting the requirement of HF in stabilizing membrane-targeted SOS1 through phospholipid-PH interaction[24] (**Fig. 5h**). The KR-EE HDPC signals were comparable to those of the shorter wild-type DPC, thereby negating the positive regulatory effect of HF domain (**Fig. 5i**). These observations collectively indicate that the HF and PH domains, through lipid interactions, cooperatively stabilize active SOS1 at the membrane.

In sum, p-FLOW results (**Fig. 5**) combined with single-molecule measurements in our SLB assays (**Figs. 2** and **3**) indicated that the flanking domains on both sides of SOS^{Cat} have evolved the ability to simultaneously dampen SOS activity in the basal

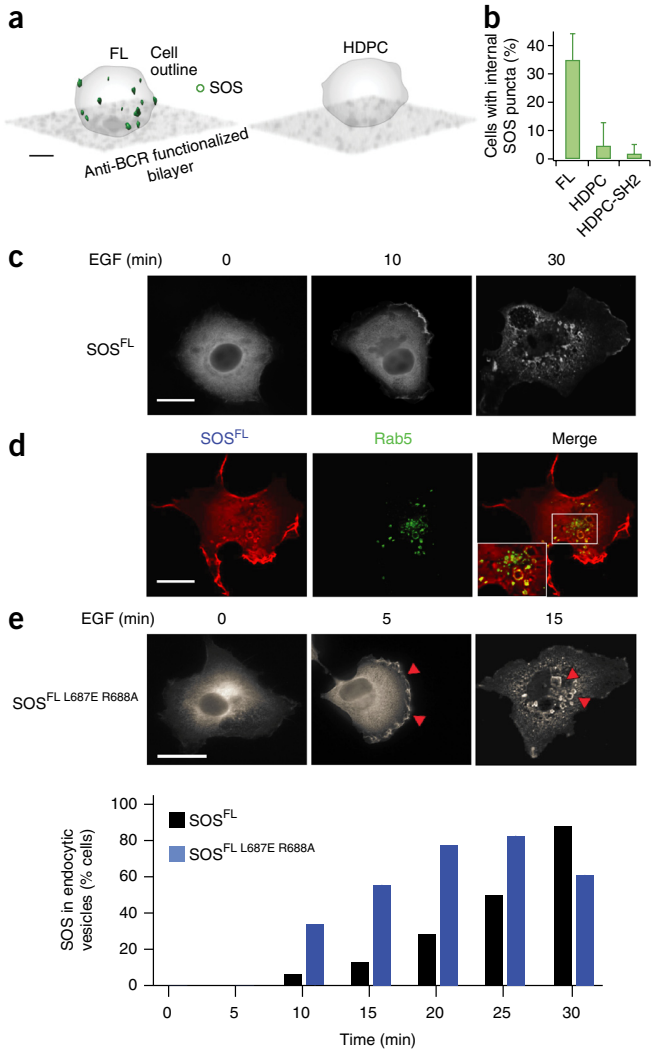

Figure 7 PR-domain-dependent SOS endocytosis mediates signal attenuation. (**a**) Confocal data in 3D rendering, showing SOS^{FL}-enriched vesicle-like structures appearing away from the cell-bilayer contact zone at late time points (~10–30 min after cell landing). Scale bar, 3 µm. (**b**) Statistics of cells displaying internal SOS puncta, as shown in **a**. Numbers of cells/SLB samples/cell cultures are: FL, 97/4/2; HDPC, 75/3/2; HDPC-SH2, 78/3/2. Error bars, s.d. across SLB samples. (**c**) Localization of EGFP-tagged $SOS1^{FL}$ in COS-1 cells stimulated with EGF for the indicated time points. Scale bar, 10 µm. (**d**) Colocalization of internalized SOS1 with the Rab5 endosomal marker in COS-1 cells stimulated for 25 min with EGF. Images shown are representative of the colocalization pattern observed in >75% of the cells in three independent experiments (25 cells analyzed per experiment). The enlarged inset in the merged image is also plotted in **Supplementary Figure 7d** as separate image channels. Scale bar, 10 µm. (**e**) Kinetics of SOS localization to endocytic vesicles in EGF-stimulated COS-1 cells. EGFP-tagged SOS^{FL} is compared with an $SOS1^{FL}$ molecule with a functionally impaired allosteric pocket ($SOS^{FL\ L687E\ R688A}$). Representative images accompany the bar graph. The results represent an average of two independent experiments (25 cells counted per condition for each experiment). Scale bar, 10 µm. Source data for plots and graphs are available online.

state but enhance SOS activity after receptor stimulation (further discussed in **Supplementary Note 3**).

Regulation of superprocessive SOS by endocytosis

SOS^{Cat}, SOS^{DPC}, and SOS^{HDPC} are all highly processive in SLB assays and in cellular p-FLOW assays are less sensitive than SOS^{FL} to attenuation at late time points of induced signaling. Interestingly, SOS^{FL} mimics these characteristics of SOS truncation when functionalized with a C-terminally grafted farnesylation signal sequence from H-Ras, which artificially targets SOS1 to the membrane[48] (**Supplementary Fig. 6**). Deletion of the Grb2-binding domain of SOS1, its putative primary mode of membrane recruitment, thus produces a molecular and cellular phenotype resembling artificial membrane targeting.

To further investigate membrane recruitment and subsequent trafficking of SOS1, we imaged SOS1-EGFP in living cells by TIRFM and spinning-disc confocal microscopy. For this experiment, we used the hybrid live-cell SLB platform[49–52] to simulate the native signaling geometry of B cells interacting with antigen-presenting cells (**Supplementary Fig. 7a**). SOS-deficient DT40 B cells expressing human SOS1-EGFP were spread on SLBs functionalized with antibody that recognizes and activates the BCR[53], thereby triggering activation of SOS[54,55] (Online Methods).

B-cell activation from the supported membrane led to formation of BCR microclusters, as observed through TIRFM imaging of a Cy5 label on the antibody (**Fig. 6a**). SOS^{FL} was efficiently recruited to sites of BCR clusters, whereas SOS^{Cat} did not colocalize with BCR clusters, although it did localize to the membrane, presumably through binding allosteric Ras (**Fig. 6a**,**b**). SOS^{HDPC} also did not colocalize with the BCR clusters (**Fig. 6b** and **Supplementary Fig. 7b**). Contrasting reports have addressed the roles of signaling complexes and SOS1 function. In our B-cell system devoid of any endogenous SOS expression, chimeric SOS^{HDPC}-SH2, with a single SH2 domain of Grb2 grafted onto SOS^{HDPC}, did not colocalize with sites of BCR microclusters (**Fig. 6b** and **Supplementary Fig. 7b**). In contrast, addition of the PR domain to SOS^{Cat} or to SOS^{DPC} enabled SOS1-BCR colocalization (**Fig. 6b**, **Supplementary Fig. 7b** and **Supplementary Note 4**).

Over time, the initially scattered BCR clusters concatenated and moved toward the center of the synapses formed between the B cells and the SLB. Approximately 15–20 min after cell landing, a large central cluster appeared, a phenomenon commonly referred to as 'BCR capping'[56] (**Fig. 6c** and **Supplementary Movie 1**). SOS^{FL} initially moved with the activated BCR, but at later time points we found that it was depleted from the central BCR cluster (**Fig. 6d**,**e**). Thus, SOS^{FL} leaves the plasma membrane at the site of the central BCR cluster, and this occurrence also correlates with attenuation of SOS^{FL}-driven Ras-ERK signaling at later time points (**Fig. 4g**). Confocal fluorescence microscopy revealed the appearance of punctate SOS structures, which were located inside the cells and were reminiscent of endocytic vesicles (**Fig. 7a**). Moreover, these vesicle-like structures appeared only for SOS^{FL} but not for SOS^{HDPC} or the chimeric SOS^{HDPC}-SH2, and only on bilayers displaying the BCR-activating antibody (**Fig. 7a**,**b**). These observations suggest that removal of SOS1 from the membrane in a BCR-signal-dependent process requires the C terminus.

To more definitively address disappearance of SOS^{FL} from the plasma membrane, we used COS-1 cells with a much larger cytoplasmic volume than that of DT40 B cells. Visualization of transfected EGFP-tagged SOS^{FL} revealed predominantly cytoplasmic and evenly distributed SOS1 before epidermal growth factor (EGF) stimulation. We observed prominent membrane recruitment of SOS1 at the plasma membrane 10 min after EGF stimulation. By 30 min after stimulation, most SOS molecules had localized to perinuclear vesicular structures (**Fig. 7c**). The vesicular SOS1 colocalized with the early endosomal marker protein Rab5 (ref. 57), thus indicating that SOS1 molecules are removed from the plasma membrane via endocytosis (**Fig. 7d**).

We found that the kinetics of SOS1 endocytosis was influenced by the allosteric Ras-binding pocket. A SOS1 mutant impaired in allosteric Ras binding ($SOS^{FL\ L687E\ R688A}$) exhibited accelerated endocytosis (**Fig. 7e**). Binding of SOS1 to Ras via its allosteric pocket thus appears to counteract the endocytosis of SOS1.

DISCUSSION

Signal propagation from receptors to the Ras pathway is commonly accepted to involve recruitment of SOS from the cytosol to the plasma membrane via the adaptor protein Grb2. In its classical interpretation, the increased membrane localization of SOS is presumed to tip the RasGEF-RasGAP balance at the membrane in favor of Ras activation, thus explaining how signals are relayed downstream. However, several results have challenged this classical model, particularly the recurring observation that SOS-truncation mutants lacking the Grb2-binding PR domain remain signaling competent in cells[29–34]. More recently, we have shown that SOS stably associates with a lipid-membrane surface by engaging Ras at the allosteric binding pocket. In reconstituted-membrane systems, this mechanism alone (i.e., independently of other mechanisms of SOS membrane anchoring) is sufficient for sustained association of SOS with the membrane, where it can processively activate thousands of Ras molecules[38]. Strikingly, essentially no dynamic equilibrium is present; membrane recruitment of SOS is quasi-irreversible at signaling-relevant timescales.

Here we demonstrated that the membrane recruitment probability of SOS by allosteric Ras is strongly accelerated by RasGTP relative to RasGDP, thereby explaining how SOS constructs lacking the Grb2-binding PR domain are capable of sensing receptor triggering. In a cellular context, RasGTP levels are primed after receptor activation, for example, because of the activity of RasGRP or other exchange factors that produce RasGTP and facilitate SOS recruitment; this process is fueled by strong positive feedback as the recruited SOS produces increasingly more RasGTP. This ability to respond to receptor stimuli independently of Grb2 is further augmented by the lipid-interacting PH and HF domains, which bind lipidic second messengers such as PIP_2 and phosphatidic acid.

In light of the spontaneous and nearly irreversible activating characteristics of SOS, the question shifts to how receptor-mediated signals maintain control of SOS via Grb2 binding. The literature abounds with apparently conflicting results on this matter. In particular, it has been unclear whether the C-terminal PR domain plays a positive, redundant, or even negative regulatory role in SOS signaling. Our p-FLOW assay, which considers the multifactorial aspects of signal transduction (i.e., expression level, pathway activity, and time after receptor stimulation), revealed that the PR domain performs dual functions in receptor-stimulated cells, acting as either a signal facilitator or a signal terminator, depending on the phase of the signaling process. In addition, the PR domain contributes to inhibition of SOS in the basal state.

From the perspective of receptor-mediated activation of SOS, Grb2 binding by the PR domain clearly increases the rate of activation. Our multiparameter mapping of the activity of the SOS-Ras-ERK cascade, enabled by reconstitution of SOS1 in SOS-deficient B cells, revealed that spontaneous activation of SOS scales with SOS expression level. Essentially, the spontaneous activation of SOS is driven by Le Chatelier's principle and is simply a probabilistic event that scales with concentration. Under endogenous expression levels, this spontaneous activation must be sufficiently slow as to be inconsequential in the context of background GAP activity, thus requiring the additional boost from receptor-mediated Grb2 recruitment to trigger a productive Ras signal (extended discussion in **Supplementary Note 5**; **Supplementary Fig. 8a–d**). We propose endocytosis as a method of signal attenuation that provides an actively regulated mechanism to remove SOS from the plasma membrane, effectively cutting off access to new Ras molecules. SOS constructs lacking the PR domain are not endocytosed, and they exhibit sustained ERK activation levels (further discussed in **Supplementary Note 6**). Thus, in its natural state, SOS activation follows a one-way trafficking circuit with active removal from the membrane via the PR domain as the shutdown mechanism.

Recently, it has become clear that single–amino acid variants in RasGEFs have a profound biological effect. We established that the EF hands in RasGRP1 play a dual role in keeping this RasGEF in the autoinhibited state while simultaneously allowing for calcium-induced activation[58]. A single–amino acid variant allele, *Rasgrp1*^{Anaef}, with a point-mutated EF hand, perturbs both regulatory roles of this domain and leads to autoimmune features in *Rasgrp1*^{Anaef} mice[59]. The structural basis for PR-domain-facilitated autoinhibition and the transition to the activated state of SOS is unknown, because efforts to produce functional full-length SOS1 protein including the PR domain have been unsuccessful to date. Mining public databases, we found several *SOS1* variants with point mutations or stop codons in the PR domain, which are linked to Noonan developmental syndrome, hyperplastic syndromes such as hereditary gingival fibromatosis[60], and various cancers (**Supplementary Fig. 8e**). It is plausible that subtle point mutations in the PR domain may have substantial biological effects and contribute to human disease.

METHODS

Methods and any associated references are available in the online version of the paper.

Note: Any Supplementary Information and Source Data files are available in the online version of the paper.

ACKNOWLEDGMENTS

The authors thank the members of the laboratories of J.P.R., J.T.G., J. Kuriyan, and D.B.-S. for helpful comments and suggestions. The authors thank J. Kuriyan for insightful comments on the manuscript. In addition, the authors thank W.-C. Lin and L. Iversen for assistance with initial SLB experiments. This research was supported by a P01 Program grant from NIH-NIAID (AI091580 – to J.P.R. and J.T.G.). Further support came from R01-CA187318 NIH-NCI and R01-AI104789 (both to J.P.R.) and ARRA stimulus supplement GM078266 (to D.B.-S. and K.K.Y.) as well as a grant from the Danish Council for Independent Research, Natural Sciences (to S.M.C.). We thank T. Kurosaki (RIKEN) for providing wild-type and $SOS1^{-2-}$ DT40 B cells.

AUTHOR CONTRIBUTIONS

S.M.C., H.-L.T., and J.E.J. performed experiments and analyzed data. S.A. and M.G.T. assisted with live-cell experiments. J.S.I. purified proteins. K.K.Y. performed COS1 cell experiments under supervision of D.B.-S. J.T.G., J.P.R., S.M.C., H.-L.T., and J.E.J. conceptualized and designed experiments. S.M.C., H.-L.T., J.E.J., J.P.R., and J.T.G. wrote the paper. J.T.G. and J.P.R. supervised the project. All authors discussed and commented on the results.

COMPETING FINANCIAL INTERESTS

The authors declare no competing financial interests.

1. Campbell, S.L., Khosravi-Far, R., Rossman, K.L., Clark, G.J. & Der, C.J. Increasing complexity of Ras signaling. *Oncogene* **17**, 1395–1413 (1998).
2. Chang, L. & Karin, M. Mammalian MAP kinase signalling cascades. *Nature* **410**, 37–40 (2001).
3. Karnoub, A.E. & Weinberg, R.A. Ras oncogenes: split personalities. *Nat. Rev. Mol. Cell Biol.* **9**, 517–531 (2008).
4. Stephen, A.G., Esposito, D., Bagni, R.K. & McCormick, F. Dragging ras back in the ring. *Cancer Cell* **25**, 272–281 (2014).

5. McCormick, F. Signal transduction: how receptors turn Ras on. *Nature* **363**, 15–16 (1993).
6. Findlay, G.M. & Pawson, T. How is SOS activated? Let us count the ways. *Nat. Struct. Mol. Biol.* **15**, 538–540 (2008).
7. Groves, J.T. & Kuriyan, J. Molecular mechanisms in signal transduction at the membrane. *Nat. Struct. Mol. Biol.* **17**, 659–665 (2010).
8. Das, J. *et al.* Digital signaling and hysteresis characterize ras activation in lymphoid cells. *Cell* **136**, 337–351 (2009).
9. Jun, J.E., Rubio, I. & Roose, J.P. Regulation of ras exchange factors and cellular localization of ras activation by lipid messengers in T cells. *Front. Immunol.* **4**, 239 (2013).
10. Egan, S.E. *et al.* Association of Sos Ras exchange protein with Grb2 is implicated in tyrosine kinase signal transduction and transformation. *Nature* **363**, 45–51 (1993).
11. Genot, E. & Cantrell, D.A. Ras regulation and function in lymphocytes. *Curr. Opin. Immunol.* **12**, 289–294 (2000).
12. Kortum, R.L. *et al.* Targeted Sos1 deletion reveals its critical role in early T-cell development. *Proc. Natl. Acad. Sci. USA* **108**, 12407–12412 (2011).
13. Baltanás, F.C. *et al.* Functional redundancy of Sos1 and Sos2 for lymphopoiesis and organismal homeostasis and survival. *Mol. Cell. Biol.* **33**, 4562–4578 (2013).
14. Wang, D.Z. *et al.* Mutation in Sos1 dominantly enhances a weak allele of the EGFR, demonstrating a requirement for Sos1 in EGFR signaling and development. *Genes Dev.* **11**, 309–320 (1997).
15. Findlay, G.M. *et al.* Interaction domains of Sos1/Grb2 are finely tuned for cooperative control of embryonic stem cell fate. *Cell* **152**, 1008–1020 (2013).
16. Buday, L. & Downward, J. Epidermal growth factor regulates p21ras through the formation of a complex of receptor, Grb2 adapter protein, and Sos nucleotide exchange factor. *Cell* **73**, 611–620 (1993).
17. Gale, N.W., Kaplan, S., Lowenstein, E.J., Schlessinger, J. & Bar-Sagi, D. Grb2 mediates the EGF-dependent activation of guanine nucleotide exchange on Ras. *Nature* **363**, 88–92 (1993).
18. Li, N. *et al.* Guanine-nucleotide-releasing factor hSos1 binds to Grb2 and links receptor tyrosine kinases to Ras signalling. *Nature* **363**, 85–88 (1993).
19. Rozakis-Adcock, M., Fernley, R., Wade, J., Pawson, T. & Bowtell, D. The SH2 and SH3 domains of mammalian Grb2 couple the EGF receptor to the Ras activator mSos1. *Nature* **363**, 83–85 (1993).
20. Waterman, H. *et al.* A mutant EGF-receptor defective in ubiquitylation and endocytosis unveils a role for Grb2 in negative signaling. *EMBO J.* **21**, 303–313 (2002).
21. Chardin, P. *et al.* Human Sos1: a guanine nucleotide exchange factor for Ras that binds to GRB2. *Science* **260**, 1338–1343 (1993).
22. Gureasko, J. *et al.* Membrane-dependent signal integration by the Ras activator Son of sevenless. *Nat. Struct. Mol. Biol.* **15**, 452–461 (2008).
23. Gureasko, J. *et al.* Role of the histone domain in the autoinhibition and activation of the Ras activator Son of Sevenless. *Proc. Natl. Acad. Sci. USA* **107**, 3430–3435 (2010).
24. Yadav, K.K. & Bar-Sagi, D. Allosteric gating of Son of sevenless activity by the histone domain. *Proc. Natl. Acad. Sci. USA* **107**, 3436–3440 (2010).
25. Margarit, S.M. *et al.* Structural evidence for feedback activation by Ras.GTP of the Ras-specific nucleotide exchange factor SOS. *Cell* **112**, 685–695 (2003).
26. Roberts, A.E. *et al.* Germline gain-of-function mutations in SOS1 cause Noonan syndrome. *Nat. Genet.* **39**, 70–74 (2007).
27. Tumurkhuu, M., Saitoh, M., Takita, J., Mizuno, Y. & Mizuguchi, M. A novel SOS1 mutation in Costello/CFC syndrome affects signaling in both RAS and PI3K pathways. *J. Recept. Signal Transduct. Res.* **33**, 124–128 (2013).
28. Kholodenko, B.N., Hoek, J.B. & Westerhoff, H.V. Why cytoplasmic signalling proteins should be recruited to cell membranes. *Trends Cell Biol.* **10**, 173–178 (2000).
29. Karlovich, C.A. *et al. In vivo* functional analysis of the Ras exchange factor son of sevenless. *Science* **268**, 576–579 (1995).
30. Corbalan-Garcia, S., Margarit, S.M., Galron, D., Yang, S.S. & Bar-Sagi, D. Regulation of Sos activity by intramolecular interactions. *Mol. Cell. Biol.* **18**, 880–886 (1998).
31. McCollam, L. *et al.* Functional roles for the pleckstrin and Dbl homology regions in the Ras exchange factor Son-of-sevenless. *J. Biol. Chem.* **270**, 15954–15957 (1995).
32. Wang, W. *et al.* The Grb2 binding domain of mSos1 is not required for downstream signal transduction. *Nat. Genet.* **10**, 294–300 (1995).
33. Zhao, C., Du, G., Skowronek, K., Frohman, M.A. & Bar-Sagi, D. Phospholipase D2-generated phosphatidic acid couples EGFR stimulation to Ras activation by Sos. *Nat. Cell Biol.* **9**, 706–712 (2007).
34. Roose, J.P., Mollenauer, M., Ho, M., Kurosaki, T. & Weiss, A. Unusual interplay of two types of Ras activators, RasGRP and SOS, establishes sensitive and robust Ras activation in lymphocytes. *Mol. Cell. Biol.* **27**, 2732–2745 (2007).
35. Chen, R.H., Corbalan-Garcia, S. & Bar-Sagi, D. The role of the PH domain in the signal-dependent membrane targeting of Sos. *EMBO J.* **16**, 1351–1359 (1997).
36. Groves, J.T., Ulman, N. & Boxer, S.G. Micropatterning fluid lipid bilayers on solid supports. *Science* **275**, 651–653 (1997).
37. Groves, J.T. & Boxer, S.G. Micropattern formation in supported lipid membranes. *Acc. Chem. Res.* **35**, 149–157 (2002).
38. Iversen, L. *et al.* Ras activation by SOS: allosteric regulation by altered fluctuation dynamics. *Science* **345**, 50–54 (2014).
39. Lin, W.C. *et al.* H-Ras forms dimers on membrane surfaces via a protein-protein interface. *Proc. Natl. Acad. Sci. USA* **111**, 2996–3001 (2014).
40. Bos, J.L., Rehmann, H. & Wittinghofer, A. GEFs and GAPs: critical elements in the control of small G proteins. *Cell* **129**, 865–877 (2007).
41. Boykevisch, S. *et al.* Regulation of ras signaling dynamics by Sos-mediated positive feedback. *Curr. Biol.* **16**, 2173–2179 (2006).
42. Hall, B.E., Yang, S.S., Boriack-Sjodin, P.A., Kuriyan, J. & Bar-Sagi, D. Structure-based mutagenesis reveals distinct functions for Ras switch 1 and switch 2 in Sos-catalyzed guanine nucleotide exchange. *J. Biol. Chem.* **276**, 27629–27637 (2001).
43. Sondermann, H. *et al.* Structural analysis of autoinhibition in the Ras activator Son of sevenless. *Cell* **119**, 393–405 (2004).
44. Kubiseski, T.J., Chook, Y.M., Parris, W.E., Rozakis-Adcock, M. & Pawson, T. High affinity binding of the pleckstrin homology domain of mSos1 to phosphatidylinositol (4,5)-bisphosphate. *J. Biol. Chem.* **272**, 1799–1804 (1997).
45. Oh-hora, M., Johmura, S., Hashimoto, A., Hikida, M. & Kurosaki, T. Requirement for Ras guanine nucleotide releasing protein 3 in coupling phospholipase C-gamma2 to Ras in B cell receptor signaling. *J. Exp. Med.* **198**, 1841–1851 (2003).
46. Jun, J.E., Yang, M., Chen, H., Chakraborty, A.K. & Roose, J.P. Activation of extracellular signal-regulated kinase but not of p38 mitogen-activated protein kinase pathways in lymphocytes requires allosteric activation of SOS. *Mol. Cell. Biol.* **33**, 2470–2484 (2013).
47. Sondermann, H., Nagar, B., Bar-Sagi, D. & Kuriyan, J. Computational docking and solution x-ray scattering predict a membrane-interacting role for the histone domain of the Ras activator son of sevenless. *Proc. Natl. Acad. Sci. USA* **102**, 16632–16637 (2005).
48. Aronheim, A. *et al.* Membrane targeting of the nucleotide exchange factor Sos is sufficient for activating the Ras signaling pathway. *Cell* **78**, 949–961 (1994).
49. Mossman, K.D., Campi, G., Groves, J.T. & Dustin, M.L. Altered TCR signaling from geometrically repatterned immunological synapses. *Science* **310**, 1191–1193 (2005).
50. Davey, A.M., Liu, W., Sohn, H.W., Brzostowski, J. & Pierce, S.K. Understanding the initiation of B cell signaling through live cell imaging. *Methods Enzymol.* **506**, 265–290 (2012).
51. Balagopalan, L., Sherman, E., Barr, V.A. & Samelson, L.E. Imaging techniques for assaying lymphocyte activation in action. *Nat. Rev. Immunol.* **11**, 21–33 (2011).
52. Grakoui, A. *et al.* The immunological synapse: a molecular machine controlling T cell activation. *Science* **285**, 221–227 (1999).
53. Weber, M. *et al.* Phospholipase C-gamma2 and Vav cooperate within signaling microclusters to propagate B cell spreading in response to membrane-bound antigen. *J. Exp. Med.* **205**, 853–868 (2008).
54. Brdicka, T. *et al.* Non-T cell activation linker (NTAL): a transmembrane adaptor protein involved in immunoreceptor signaling. *J. Exp. Med.* **196**, 1617–1626 (2002).
55. Janssen, E., Zhu, M., Zhang, W., Koonpaew, S. & Zhang, W. LAB: a new membrane-associated adaptor molecule in B cell activation. *Nat. Immunol.* **4**, 117–123 (2003).
56. Pierce, S.K. & Liu, W. The tipping points in the initiation of B cell signalling: how small changes make big differences. *Nat. Rev. Immunol.* **10**, 767–777 (2010).
57. Stenmark, H. Rab GTPases as coordinators of vesicle traffic. *Nat. Rev. Mol. Cell Biol.* **10**, 513–525 (2009).
58. Iwig, J.S. *et al.* Structural analysis of autoinhibition in the Ras-specific exchange factor RasGRP1. *eLife* **2**, e00813 (2013).
59. Daley, S.R. *et al.* Rasgrp1 mutation increases naive T-cell CD44 expression and drives mTOR-dependent accumulation of Helios$^+$ T cells and autoantibodies. *eLife* **2**, e01020 (2013).
60. Rojas, J.M., Oliva, J.L. & Santos, E. Mammalian son of sevenless guanine nucleotide exchange factors: old concepts and new perspectives. *Genes Cancer* **2**, 298–305 (2011).

ONLINE METHODS

Proteins and reagents. H-Ras$^{C118S\ C181}$ (H-Ras construct containing residues 1–181 with a single cysteine at position C181 used for coupling to the bilayer, termed Ras herein), SOS^{Cat} Cys-lite (residues 566–1049 with the following mutations: C838A, C635A, C980S, and E718C), SOS^{DPC} (residues 198–1049), SOS^{HDPC} (residues 1–1049), and SOS$^{HDPC\ R552G}$ (residues 1–1049 with R552G) of human SOS1 were expressed in *Escherichia coli* and purified as previously described[22]. Lipids were purchased from Avanti. TR-DHPE, BODIPY-GDP, and BODIPY-GTP were purchased from Invitrogen. ATTO 647N–maleimide, ATTO 488–labeled guanosine diphosphate (EDA–GDP–ATTO 488) and EDA–GppNp–ATTO 488 (nonhydrolyzable analog of GTP were purchased from Jena Bioscience. GTP was purchased from Sigma-Aldrich, and GDP was purchased from MP Biomedicals. Biotinylated anti-chicken IgM was purchased from Sigma (SAB3700240), and Cy5-labeled streptavidin was from Life Technologies (43-4316). Validation information for commercial antibodies is available on the manufacturers' websites.

Protein labeling and benchmarking. SOS constructs were fluorescently labeled by reaction of 1:10 molar ratio of unlabeled protein with ATTO 647N–maleimide for 2 h at 23 °C. Unreacted fluorophores were removed with PD-10 columns (GE Healthcare). The degree of labeling was determined by UV-vis spectroscopy (NanoDrop 2000, Thermo Scientific), yielding 90% for SOS^{Cat} Cys-lite, 119% for SOS^{DPC}, 106% for SOS^{HDPC}, and 118% for SOS$^{HDPC\ R552G}$. SOS^{DPC}, SOS^{HDPC} and SOS$^{HDPC\ R552G}$ contained multiple cysteines, thus explaining why labeling efficiencies exceeded 100%.

Dye labeling can potentially alter protein behavior, and caution is always needed in the interpretation of related results. Here, nucleotide-exchange experiments were conducted to ascertain that labeling did not alter enzyme behavior; comparison of unlabeled and labeled constructs in the stopped-flow assay indicated that labeling had a negligible effect on the *in vitro* activity of SOS in our system (**Supplementary Fig. 1c**).

Ras-decorated supported lipid bilayers for *in vitro* assays. Ras-decorated bilayers were prepared as previously described[22,38]. Lipids dissolved in chloroform were mixed in a round-bottomed flask. Solvent was evaporated by rotary evaporation (40 °C, 10 min) followed by N_2 flow (20 min). Small unilamellar vesicles (SUVs) were formed by rehydration of the dried lipid film in PBS (pH 7.45). The vesicle suspension was extruded 11 times (Avestin Miniextruder, 30-nm-pore-diameter polycarbonate membranes; Millipore). The lipid composition was 3% DOPS, 3% MCC-DOPE, 0.01% TxRed-DHPE, and the remainder Egg-PC.

SLBs were formed by incubation of the SUV suspension for 30 min on cleaned piranha-etched glass slides mounted in flow chambers (FCS2 flow chambers, Bioptechs). The sample was incubated with casein in PBS (2.5 mg/ml) for 10 min and was then incubated for 2.5 h with Ras in PBS (1 mg/ml). After Ras incubation, unreacted MCC was quenched by treatment with 2-β-mercaptoethanol in PBS (5 mM) for 10 min. A motorized syringe pump (PHD 2000, Harvard Apparatus) was used throughout the sample preparation for liquid injections and washing steps.

For loading of fluorescent nucleotide onto Ras, samples were equilibrated at 4 °C and washed with 3 mL loading buffer (40 mM HEPES and 150 mM NaCl, pH 7.4); the native nucleotide bound to Ras was stripped in a 20-min incubation with EDTA in loading buffer (50 mM EDTA, 40 mM HEPES, and 150 mM NaCl, pH 7.4). This step was immediately followed by overnight incubation of samples with 10 μM fluorescent nucleotide analog in reaction buffer (40 mM HEPES, 100 mM NaCl, and 5 mM MgCl, pH 7.4). Fluorescent nucleotides used in this study included BODIPY-GDP, BODIPY-GTP, ATTO 488–GDP, and ATTO 488–GppNp. A control experiment in which samples underwent all steps except Ras incubation showed no detectable nonspecific binding of the applied fluorescent nucleotides to the SLB.

Immediately before microscopy, samples were brought to room temperature, and any unbound fluorescent nucleotide was removed by washing with 3 mL reaction buffer (40 mM HEPES, 100 mM NaCl, 5 mM $MgCl_2$, and 1 mM TCEP, pH 7.4) under constant flow. The two-dimensional fluidity of lipids and Ras was confirmed for each sample with fluorescence recovery after photobleaching (FRAP).

Antibody-functionalized supported lipid bilayers for live-cell imaging. Bilayers for live-cell experiments were prepared as described above, with a lipid composition of 5% DOPS, 0.1% biotinyl cap PE, 0.005% TxRed-DHPE, and the remainder Egg-PC. A piranha-etched glass slide (1, Fisher Scientific) mounted in a microscopy chamber (A-7816, Life Technologies) was incubated with SUV suspension (1 mg/mL) for 30 min. The sample was then treated with Cy5-labeled streptavidin (18.8 nM) for 30 min and was then incubated with biotinylated anti-chicken IgM (62 nM; SAB3700240, Sigma) for 30 min. Each incubation step was followed by copious washing with PBS.

Stopped-flow supported lipid bilayer assay. Labeled and unlabeled SOS constructs were mixed at the desired ratio (typically 1:20) at a total concentration of 100 nM and flowed over the bilayer as a transient pulse. The number of labeled SOS molecules remaining on the bilayer after the pulse (due to capture by catalytic Ras in the absence of free nucleotide)[30,40] was counted at the single-molecule level and used to infer the recruitment probability (**Supplementary Note 7**). We experimentally confirmed that SOS in our system was indeed stably tethered to the bilayer via Ras in the absence of free nucleotide. For Y64A experiments, SOS engaged the membrane in a transient manner (**Fig. 2c**), and the extent of binding was inferred from the observed peak binding during the SOS pulse instead of from the plateau (data in **Fig. 2d**).

The nucleotide-exchange reaction was initiated by providing a continuous flow of nucleotide (120 μM GDP or GTP). SOS desorption and nucleotide-exchange kinetics were quantified at different time points by acquisition of an image of the fluorescent nucleotide on Ras and ten images of the labeled SOS. For each time point, we imaged a different position in the flow chamber to avoid bleaching. The ten images of SOS at each position allowed us to discard immobile SOS in the analysis (i.e., SOS bound to defects in the bilayer). This is a crucial aspect of the experimental design because it avoids bias from sample-to-sample variation in the number of defects as well as possible differential tendencies of various protein constructs to adhere to bilayer defects. By counting membrane-bound SOS through single-molecule tracking, we were able to focus entirely on species that are laterally mobile.

A clear demonstration that the assay probed specific interactions between Ras and SOS came from the observation that all SOS constructs tested exhibited sensitivity to the nucleotide state of Ras with consistently increased recruitment probability as well as a prolonged residency period on membranes displaying RasGTP (**Fig. 2d** and **Supplementary Fig. 3a–c**).

For specific comparison of desorption for successfully activated SOS constructs (**Fig. 3c**), traces were normalized to the SOS count at the membrane observed at the initiation of the nucleotide chase. For SOS^{Cat}, we observed a fraction of rapidly desorbing species during the first few seconds of the chase (**Fig. 2c**). This fast-desorbing fraction did not contribute to processive Ras turnover (**Supplementary Fig. 1d**), and for the comparisons with other constructs (**Fig. 3c** and **Supplementary Fig. 3b**,**c**), we cropped the first 10 s of the trace.

Maintenance and transfection of DT40 and Jurkat cell lines. Culture maintenance, plasmid transfection, and BCR stimulation of chicken DT40 B cell lines were carried out as previously described[46]. Jurkat cell culture and transfection techniques were also performed as previously described[8]. The SOS1$^{-/-}$2$^{-/-}$ DT40 B cells were generated in T. Kurosaki's laboratory (RIKEN). Both wild-type and SOS1$^{-/-}$2$^{-/-}$ DT40 B cells were gifts from T. Kurosaki. The obtained cell lines were confirmed to be free of mycoplasma contamination. For routine cell functional authentication, surface expression of B-cell receptor (BCR) was confirmed by flow cytometry and by BCR-induced pERK2 measurement similar to the experiment shown in **Supplementary Figure 4**. Jurkat T cells were obtained from the ACCC and were maintained according to the provided guidelines.

To generate EGFP-tagged hSOS1 variants, EGFP coding sequence (CDS) was PCR-amplified with Xba I- and Not I-flanked primers from pEGFP-N1 plasmid (Clontech). The resulting SOS1-EGFP construct bears a five–amino acid linker (SRGGR) between SOS1 and EGFP CDS. Expression was confirmed by western blotting with anti-GFP antibody (Cell Signaling, 2956) (**Supplementary Fig. 4a**).

Live-cell imaging. For live-cell microscopy, 2.5 million cells were exchanged from cell culture medium to 1 mL of serum-free RPMI by pelleting cells through 5-min centrifugation at 500*g*; this was followed by 30-min incubation in serum-free RPMI at 37 °C. Cells were imaged in pH 7.40, 10 mM HEPES, 68 mM NaCl, 2.5 mM KCl, 0.35 mM Na_2HPO_4, 3 mM D-glucose, 1 mM $CaCl_2$, 2 mM $MgCl_2$, and 0.1% BSA.

doi:10.1038/nsmb.3275

Live-cell imaging was performed with a stage-top incubator and an objective heater (Chamlide TC-A, Quorum Technology). Experiments were initiated by addition of cells to SLBs functionalized with anti-BCR (Sigma, SAB3700240). The bilayer was heated to 37 °C before addition of cells. The 488-nm channel was used for SOS-EGFP, and the 640-nm channel was used for BCR-engaged antibody on SLBs. For a few selected cells, TIRF images were acquired every ~1–5 min to follow the kinetics of the signaling reaction. Approximately 30 min after cells were added to the chamber, 488-nm and 640-nm TIRF, together with bright field and RICM micrographs were acquired at a number of positions in the microscope chamber.

Flow cytometry and data analysis. Jurkat T cells were transiently transfected for 20 h with 10 µg of wild-type or allosteric mutant (W729E) SOS^{Cat}-encoding plasmid together with 10 µg of GFP plasmid. The activity of the Ras-ERK pathway was measured by FACS staining of surface CD69 (sCD69, BD Pharmingen, 555531) together with GFP intensity measurements. GFP-positive cells were subgated into nine fractions. The geometric mean fluorescence of CD69 was determined for each fraction.

For quantitative and qualitative assays of the RAS-ERK signal module, intracellular staining of BCR-induced ERK phosphorylation was performed according to established procedures[46]. In brief, cells were stimulated with BCR cross-linking mouse IgM (clone M4, Southern Biotech, 8300-01) for the desired time period. Stimulation was then stopped by addition of 4% paraformaldehyde-PBS, and cells were fixed for 20 min at room temperature. Fixed cells were washed three times with FACS wash buffer (PBS, 1% BSA, and 10 mM EDTA) and subsequently permeabilized with prechilled 90% methanol overnight. Cells were then washed three times with FACS wash buffer and stained for pERK with rabbit antisera (Cell Signaling, 9101). pERK was visualized by secondary staining with goat anti-rabbit IgG conjugated with APC (Jackson Immunochemicals, 711-136-152).

For FACS acquisition, a minimum of 100,000 events were collected for each time point with a FACSCalibur machine (BD) and analyzed with FlowJo software. For analysis of ERK activation, cells were sorted into nine bins of equal intervals according to their SOS expression level. Subsets with fewer than 100 acquired events were disregarded for fair comparison of SOS1 variants with different expression levels.

COS1 cell transfections and immunofluorescence staining. COS1 cells were cultured and treated as previously described[22]. COS1 cells were obtained from ACCC. In brief, cells grown on cover slips were transfected with either the pCGT-T7-SOS^{Cat} or $SOS^{Cat\text{-}L687ER688A}$ construct together with GFP-tagged H-$Ras^{A59G\ D38E}$–encoding plasmid. After 24 h, transfected cells were fixed in 3.7% (v/v) formaldehyde and permeabilized with 0.1% (v/v) Triton X-100. Expressed SOS proteins were visualized by staining with anti-T7 antibody (EMD Millipore, AB3790), followed by rhodamine-conjugated anti-mouse antibody (Cappel, R-6393). Rab5 protein was expressed as a GFP-fusion protein. EGF was obtained from Invitrogen. Imaging was conducted on a Zeiss Axiovert 200M microscope.

Optical microscopy platforms. Epifluorescence and total internal reflection fluorescence microscopy was performed on a Nikon Eclipse Ti inverted microscope with a Nikon Apo TIRF 100× oil immersion objective (1.49 NA) and an EMCCD camera (Andor iXon 597DU). A mercury arc lamp was used for epifluorescence illumination. 488-nm (Sapphire HP; Coherent) and 647-nm (RCL-050-640; Crystalaser) lasers were used for through the objective TIRF imaging. Band-pass emission filters for 488- and 647-nm TIRF images were HQ515/30 and HQ700/75 (Chroma Technology), respectively. The microscope was operated with MetaMorph software (Molecular Devices).

For live-cell experiments, an additional TIRF setup was used with the following specifications: inverted microscope body (Nikon Eclipse Ti (Ti HUBC/A), Technical Instruments) equipped with a Nikon Apo TIRF 100x oil objective (1.49 NA). The microscope had a custom-built laser launch with 488-nm, 561-nm, and 633-nm lasers (all from the OBIS product line, Coherent) controlled via a laser control module (OBIS scientific remote). The TIRF setup was operated through the objective mode, and images were collected on an EMCCD (iXon ultra 897, Andor). The microscope was controlled with µManager[61].

Confocal microscopy was performed on a custom-built spinning-disk confocal system[62]. Briefly, images were captured with a Nikon Apo TIRF 100× oil-immersion objective (1.49 NA) and an EMCCD (Andor iXon3 888), and the microscope was controlled with µManager[61]. The axial slice step size was 0.5 µm.

Data analysis. A detailed description of the data analysis procedures relating to imaging experiments can be found in **Supplementary Note 7**.

Code availability. Supplementary Note 7 provides a detailed description of the data analysis procedures that can be implemented in a given coding language.

61. Edelstein, A., Amodaj, N., Hoover, K., Vale, R. & Stuurman, N. Computer control of microscopes using µManager. *Curr. Protoc. Mol. Biol.* **92**, 14.20 (2010).
62. Greene, A.C. *et al.* Spatial organization of EphA2 at the cell-cell interface modulates trans-endocytosis of ephrinA1. *Biophys. J.* **106**, 2196–2205 (2014).